

## Modeling and simulation for PV, Fuel cell Based MICROGRID under Unbalanced Loading Conditions

T. Venugopal<sup>1</sup>, B. Bhavsingh<sup>2</sup>, D. Vani<sup>3</sup>

<sup>1</sup>(Electrical And Electronics Engineering, Vaagdevi College Of Engineering, Jntuh, Ap)

<sup>2</sup>(Electrical And Electronics Engineering, Jayamukhi Institute Of Technological Sciences, Jntuh, Ap)

<sup>3</sup>(Electrical And Electronics Engineering, Vaagdevi College Of Engineering, Jntuh, Ap)

**Abstract:** Distributed generation has attracted great attention in recent years, thanks to the progress in new-generation technologies and advanced power electronics. The Microgrid has been a successful example by integrating various generation sources with the existing power distribution network through power electronic converters. This paper proposes a PV, Fuel cell based microgrid and a new control strategy for the islanded operation of a multi-bus medium voltage (MV) microgrid. The proposed control strategy of each DG comprises a proportional resonance (PR) controller with an adjustable resonance frequency, a droop control strategy, and a negative-sequence impedance controller (NSIC). The PR and droop controllers are, respectively, used to regulate the load voltage and share the average power components among the DG units. The NSIC is used to effectively compensate the negative-sequence currents of the unbalanced loads and to improve the performance of the overall microgrid system. Moreover, the NSIC minimizes the negative-sequence currents in the MV lines and thus, improving the power quality of the microgrid. The performance of the proposed control strategy is verified with PV, Fuel cell inputs by using digital time-domain simulation studies in the MATLAB/SIMULINK software environment

**Key words:** Distributed generation, medium voltage (MV) microgrid, negative-sequence current, power sharing, unbalance load, voltage control.

### I. Introduction

MEDIUM voltage (MV) microgrids will play a major role in controlling of distribution network in the future smart grids. The role of MV microgrids is more important when considering the environmental issues and economical, social, and political interests. The recently presented concept of multi-microgrids is a motivation for proposing the concept of the higher voltage level structure of microgrids, e.g., MV level A multi-microgrid consists of low voltage (LV) microgrids and distributed generation (DG) units connected to several adjacent MV feeders. Many innovative control techniques have been used for power quality enhanced operation as well as for load sharing. A microgrid that supplies to a rural area is widely spread and connected to many loads and DGs at different locations. In general, a DG may have local loads that are very close to it. There may be loads that are not near to any of the DGs and they must be shared by the DGs and the utility. These are termed as common load in this paper. The most common method of local load sharing is the droop characteristics. Parallel converters have been controlled to deliver desired real and reactive power to the system. Local signals are used as feedback to control the converters, since in a real system, the distance between the converters may make an inter-communication impractical. The real and reactive power sharing can be achieved by controlling two independent quantities – the power angle and the fundamental voltage magnitude This paper presents a new control strategy for an islanded microgrid consisting of several dispatchable electronically-interfaced three-wire DG units. The microgrid consists of several buses and operates in an MV level. Each DG unit supplies the local and nonlocal loads which can be unbalanced. The overall microgrid is controlled based on the decentralized control strategy, i.e., each DG unit is considered as a subsystem equipped with the proposed control strategy. However, it is assumed that each nonlocal bus (feeder) is equipped with a phase measurement unit (PMU) which transmits the phasor information of the feeder to the adjacent DG units. The proposed control strategy of each DG comprises a voltage control loop, a droop controller and a negative-sequence output impedance controller. The voltage controller adaptively regulates the load voltage using a PR controller. The average power sharing between the DG units is carried out by the droop controller. However, the droop controller is not able to share the negative-sequence current resulting from the unbalanced loads. Thus, a new control strategy is proposed in this paper to efficiently share the negative-sequence current among the DG units. The proposed

negative-sequence current controller adjusts the negative-sequence output impedance of its own DG such that the negative-sequence currents of the MV lines will be minimized.

## II. Modeling of PV and Fuel Cell System

The strategy of modeling a PV module is no different from modeling a PV cell. It uses the same PV cell model (Odeh I, *et al.*, 2006). The parameters are the all same, but only a voltage parameter (such as the open circuit voltage) is different and must be divided by the number of cells. The model consists of a current source ( $I_{ph}$ ), a diode (D), and a series resistance ( $R_{se}$ ). The effect of parallel resistance ( $R_{pa}$ ) is very small in a single module, thus the model does not include it. To make a better model, it also includes temperature effects on the short-circuit current ( $I_{sc}$ ) and the reverse saturation current of diode (Mezghanni D, *et al.*, 2007). It uses a single diode with the diode ideality factor ( $n$ ) set to achieve the best I-V curve match.

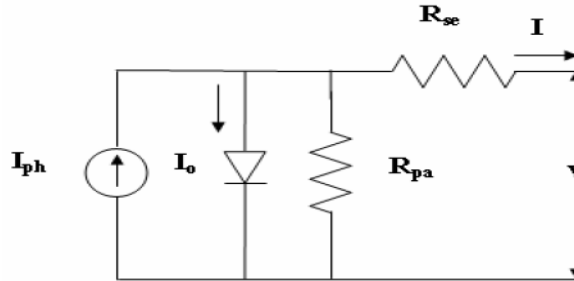


FIG 2.1 Equivalent circuit of PV cell

The below figure shows the I-V characteristics for the PV cell modeled in MATLAB. The curves are plotted with different radiations of sun from 0.25 to 1

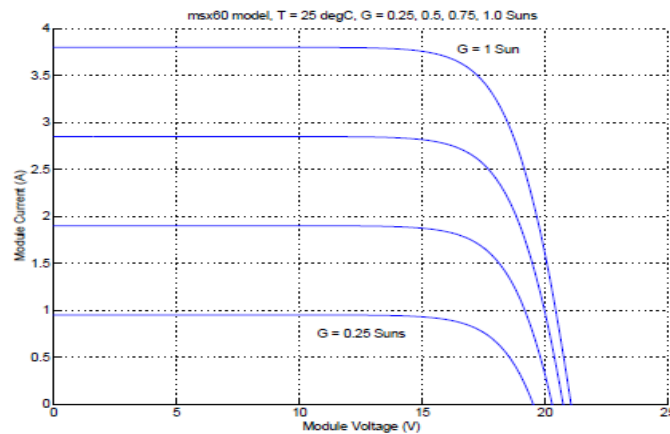


Fig.2.2 I-V characteristics of PV cell

The below figure shows the characteristics of PV module at different temperatures ranging from 25°C to 100°C. These curves match the practical characteristics of PV cells which shows that simulated model is truly working.

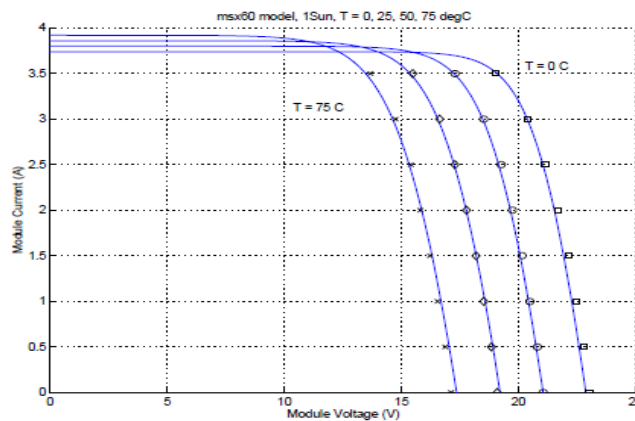


Fig.2.3 I-V characteristics with varying temperature

### III. Multi-Bus MV Microgrid Structure

Fig. 1 shows a single-line diagram of a multi-bus MV microgrid which is composed of a 20-kV three-feeder distribution system and two electronically-coupled three-wire DG units. A combination of balanced and unbalanced loads are supplied through three radial

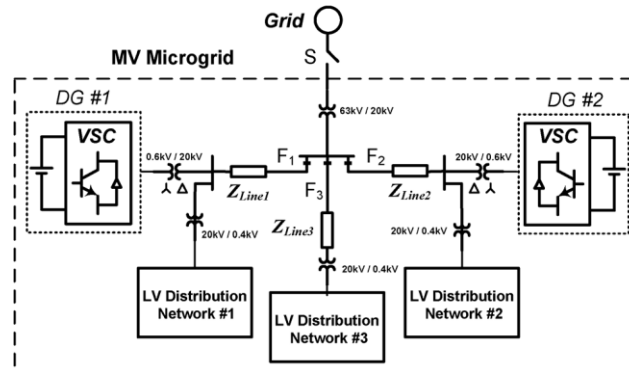


Fig.1. MV multi-bus microgrid consisting of two DG Unit

Feeders, F1, F2, F3. The DG units are connected to feeders F1, F2 through step-up transformers and are assumed to be dispatchable. Thus, each DG unit can supply any amount of the real/reactive power within the pre-specified limits. Moreover, each DG must control its own power in a decentralized control manner. The loads are connected to the MV feeders via Y/Δ transformers, and therefore, the loads do not absorb any zero-sequence current from the MV feeders. Nevertheless, the load current can assume the negative-sequence component. In this paper, it is assumed that the microgrid system operates in the islanded mode. Therefore, the DG units are responsible for compensating the negative-sequence current of the unbalanced loads. The microgrid parameters are given in Table I.

### IV. Dynamic Model of a Three-Wire Dg Unit

Each DG unit including its series and capacitive (LC) filters can be considered as a subsystem of the microgrid. To control the microgrid using the a decentralized control strategy, it is required that the dynamic model of each subsystem be derived first. Thus, in this section, the dynamic model of a three-wire DG unit, as a subsystem of the overall microgrid, is presented. Fig. 2 shows the circuit diagram of a three-wire DG subsystem. The objective is to design a feedback control system to robustly regulate the load voltages in the presence of disturbances. It should be noted that since the microgrid system is a three-phase three-wire system, the zero-sequence of the currents become zero. Thus, using the Clarke transformation, the state space equation of the system in the stationary reference frame is obtained as follows [16]:

TABLE I  
Microgrid System Parameters

Parameter	Value	Comments
$S_{base}$	2.5 MVA	DG ratings
$Z_{line1}$	$0.7 + j 1.57 \Omega$	5.7 km overhead line
$Z_{line2}$	$0.5 + j 1.25 \Omega$	4 km overhead line
$Z_{line3}$	$0.1 + j 0 \Omega$	2 km underground cable
$L_{f1}, L_{f2}$	0.3 mH	series filter inductance
$R_{f1}, R_{f2}$	0.0015 $\Omega$	series filter resistance
$C_{f1}, C_{f2}$	2200 $\mu F$	filter capacitance
$V_{dc}$	1500 V	dc bus voltage
$f_s$	2 kHz	switching frequency
$P_{max DG1}, P_{max DG2}$	2.5 MW	
$Q_{max DG1}, Q_{max DG2}$	1.5 MVA <sub>r</sub>	
$m_{DG1}, m_{DG2}$	0.333 Hz/MW	P-f droop coefficients
$n_{DG1}, n_{DG2}$	0.0245 kV/MVA <sub>r</sub>	Q-V droop coefficients
$I_{max DG1}^-$	0.3 kA	
$I_{max DG2}^-$	0.5 kA	

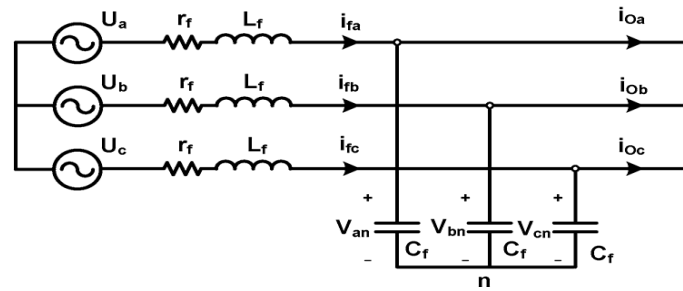


Fig. 2. Circuit diagram of a three-phase, three-wire DG unit.

$$\dot{\mathbf{X}} = \mathbf{A}\mathbf{X} + \mathbf{B}\mathbf{U} + \mathbf{E}\mathbf{W}, \quad \mathbf{Y} = \mathbf{C}\mathbf{X} \quad (1)$$

where  $\mathbf{X} = [v_\alpha, v_\beta, i_{f\alpha}, i_{f\beta}]^T$ ,  $\mathbf{U} = [U_\alpha, U_\beta]^T$ ,  $\mathbf{W} = [i_{o\alpha}, i_{o\beta}]^T$ ,  $\mathbf{Y} = [v_\alpha, v_\beta]^T$  and

$$\mathbf{A} = \begin{bmatrix} 0 & 0 & \frac{1}{C_f} & 0 \\ 0 & 0 & 0 & \frac{1}{C_f} \\ -\frac{1}{L_f} & 0 & -\frac{r_f}{L_f} & 0 \\ 0 & -\frac{1}{L_f} & 0 & -\frac{r_f}{L_f} \end{bmatrix}, \quad \mathbf{B} = \begin{bmatrix} 0 & 0 \\ 0 & 0 \\ \frac{1}{L_f} & 0 \\ 0 & \frac{1}{L_f} \end{bmatrix}$$

$$\mathbf{E} = \begin{bmatrix} -\frac{1}{C_f} & 0 \\ 0 & -\frac{1}{C_f} \\ 0 & 0 \\ 0 & 0 \end{bmatrix}, \quad \mathbf{C} = \begin{bmatrix} 1 & 0 & 0 & 0 \\ 0 & 1 & 0 & 0 \end{bmatrix}. \quad (2)$$

$$V_{\alpha\beta}(s) = G_{(2 \times 2)}(s)U_{\alpha\beta}(s) - Z_{(2 \times 2)}(s)I_{o\alpha\beta}(s) \quad (3)$$

The (1) in the Laplace domain is

where  $G_{(2 \times 2)}$  and  $Z_{(2 \times 2)}(s)$  are

$$g_{12}(s) = g_{21}(s) = z_{12}(s) = z_{21}(s) = 0$$

$$g_{11}(s) = g_{22}(s) = \frac{1}{L_f C_f s^2 + r_f C_f s + 1}$$

$$z_{11}(s) = z_{22}(s) = \frac{L_f s + r_f}{L_f C_f s^2 + r_f C_f s + 1}. \quad (4)$$

Equation (4) shows that the matrix transfer function of the DG subsystem is diagonal (completely decoupled) and can be viewed as two SISO control systems.

### V. Operation Principles of the Proposed Control Strategy

The proposed control strategy comprises 1) a voltage control, 2) a power sharing control loop, and 3) a negative-sequence current controller. The purpose of the voltage control loop is to keep the voltage of each bus of the microgrid within the acceptable limits. To eliminate the impact of the unknown dynamics (load dynamics), a feed forward controller is incorporated in the voltage control loop. In the  $\alpha\beta$ -frame, the reference signals are sinusoidal, and therefore, a PR controller is designed to ensure the excellent reference tracking [17], [18]. Moreover, since the frequency is determined by the droop control strategy and may deviate from its rated value, the proposed PR controller should adaptively adjust its parameters.

When the load is unbalanced, its power components will be oscillatory [19]. In this case, the conventional droop controller is used for sharing the average power components of the loads and a negative-sequence output impedance control strategy is proposed to effectively share the oscillatory portions of the load power. It should be noted that each DG unit mainly compensates the oscillatory power of its local load. However, the oscillatory power components of the nonlocal loads are shared among all DG units. Therefore, the proposed control strategy improves the power quality of the overall microgrid. In the following sections, the control design procedure is explained in detail.

**A .Proportional Resonance Controller with Non-Fixed Resonance Frequency**

Since the matrix transfer function of the DG subsystem in the  $\alpha\beta$ - frame is diagonal, two identical SISO controllers can be independently designed for the quadrature axes and. Fig. 3 shows the block diagram of the voltage controller for  $\alpha$  or  $\beta$  which is used to increase the internal stability and to protect the voltage source converter (VSC) of the DG unit. The gain of the proportional controller is set such that the damping factor of the dominant poles of the inner loop system becomes 0.7. In this case, the gain is set to 2.9. The reference signal for the inner Loop is generated by the PR controller as shown in Fig. 3.The PR controller is designed using the SISO tools of MATLAB software. The designed controller provides good robust stability margins for the overall closed loop system, i.e., the phase and gain margins are 46 and 8 dB. The PR controller can be considered as a series connection of a fixed part  $C(s)$  and a parameter dependent part  $C_{AD}(s)$  as

$$C(s) = \frac{5756(s + 40)(s^2 + 400s + 200,000)}{(s^2 + 4,000s + 8,000,000)},$$

$$C_{AD}(s) = \frac{1}{s^2 + 2\omega_{cut}s + \omega^2} \tag{5}$$

Based on the internal model control (IMC) theory, zero steady State tracking error for a sinusoidal reference signal is achieved if the parameter equals the frequency of the reference signal  $V_{ref}$ . The frequency of the reference signal is determined by the droop controller and may slightly drift from its nominal value Thus, the transfer function  $C_{AD}(s)$  is implemented such that the parameter can adaptively be adjusted, as shown in Fig. 4.

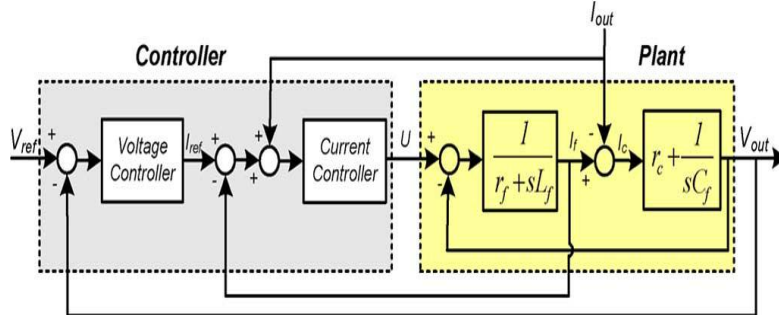


Fig. 3. Voltage controller structure in the or axis.

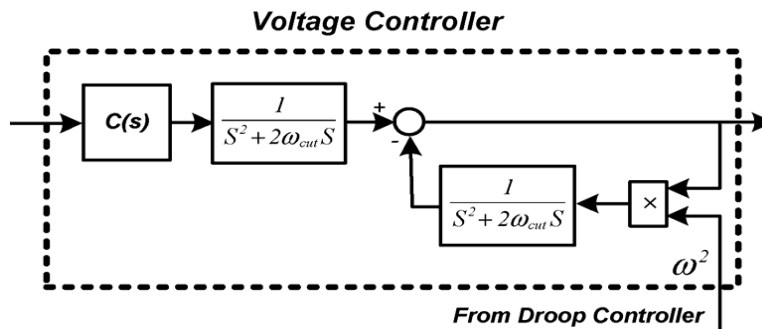


Fig. 4. Block diagram of the proposed PR controller.

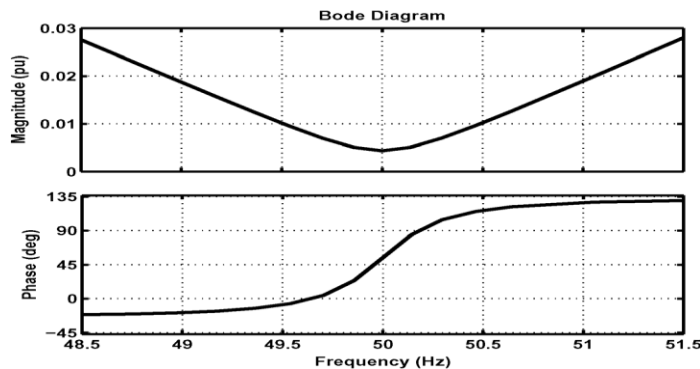


Fig. 5. Output impedance of the closed-loop DG system

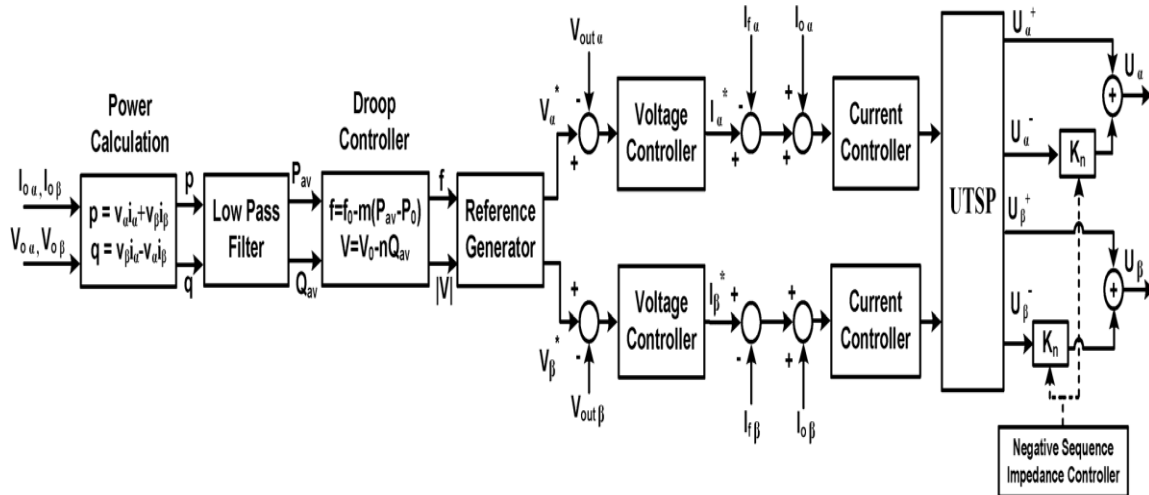


Fig. 6. Structure of the proposed control system

In this case, an excellent tracking is achieved even if the frequency of the reference signal deviates from its rated value. The damping factor  $\omega_{ut} > 0$  is a very small number whose role will be explained in Section V-D. The output impedance of the DG is defined as

$$Z_{out}(s) = - \left. \frac{V_{out}(s)}{I_{out}(s)} \right|_{V_{ref}(s)=0} \quad (6)$$

Where  $I_{out}$  and  $V_{out}$  are the terminal current and output voltage of the DG, respectively. Fig. 5 shows the frequency response of  $Z_{out}$  for the frequency interval [49 Hz, 51 Hz]. Note that the output impedance is computed for the closed-loop system according to Fig. 3 and (6). As shown in Fig. 5, the variation of  $Z_{out}$  is significant around 50 Hz. Thus, if the conventional PR controller with a fixed central frequency  $\omega$  is used, the output impedance will be increased due to the frequency drift imposed by the droop controller. However, the proposed PR controller with an adjustable resonance frequency dynamically sets its central frequency to keep the output impedance at its minimum value.

**B . Proposed Control System**

Fig. 6 shows the block diagram of the proposed control system. The voltage controllers consist of two identical PR controllers whose reference signals are The averaged power components are then applied to the droop controller to calculate frequency and voltage magnitude of the reference signals. The reference generator unit generates the reference signals for the PR controller. The outputs of the voltage controllers are considered as the reference signals for the current controllers. These signals are compared with the Currents of the series filter and are added with the feed forward signals  $i_{0a}$  and  $i_{0b}$  the resultant signals are then applied to the current controllers to generate the control signals  $U_a$  and  $U_b$ . To share the negative-sequence currents among the DG units, the signals  $U_a$  and  $U_b$  are decomposed into the symmetrical Components using the unified three-phase signal processor (UTSP) proposed in [21]. The instantaneous negative-sequence components of the control signals are multiplied by a DC gain  $K_n$  which is generated by the NSIC. In this case, the negative-sequence output impedance of each DG is adjusted by manipulating the gain  $K_n$ . The positive- and negative-sequence components of the control signals are finally summed up to generate the control signals for the gating signal generator of the VSC.

**C. Positive- and Negative-Sequence Models of Microgrid**

To obtain the positive- and negative-sequence models of the overall microgrid, the dynamic model of each DG unit is obtained in the positive- and negative-sequence frames using Fig. 6. The positive-sequence voltages of the closed-loop system in the  $\alpha\beta$ -frame can be expressed as

$$V_{\alpha,\beta}^+(s) = H(s)V_{\alpha,\beta}^*(s) - Z_{out}^+(s)I_{0\alpha,\beta}^+(s) \quad (7)$$

The negative-sequence voltages of the closed-loop system is expressed as



$$V_{\alpha,\beta}^-(s) = -Z_{out}^-(s)I_{o_{\alpha,\beta}}^-(s) \quad (8)$$

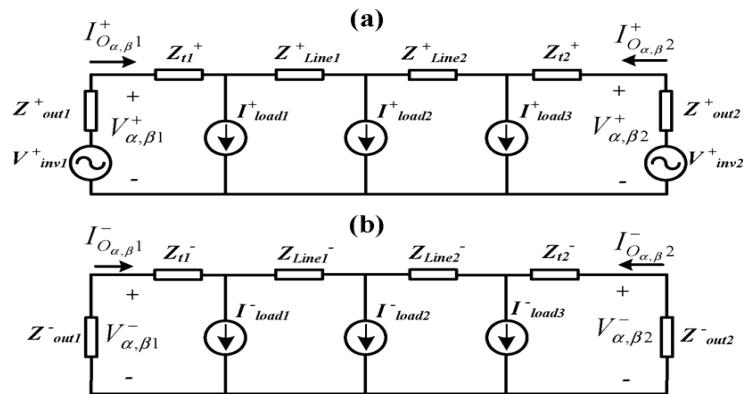


Fig. 7. (a) Positive- and (b) negative-sequence models of the two DG microgrid of Fig. 1.

Based on (7) and (8), the positive- and negative sequence models of the DG units of Fig. 1 are obtained, as shown in Fig. 7. The line and transformer parameters of both positive- and negative-sequence models are identical, and each load is modeled by a current source.

### C. Negative-Sequence Current Sharing Strategy

To optimally share the negative-sequence currents between the DG units, the negative-sequence output impedance of each DG is adjusted by the parameter  $K_n$  [Figs. 6 and 7(b)]. The studies show that the negative-sequence output impedance is inversely proportional to  $K_n$  and increases as  $\omega_{cut}$  is increased (Fig. 8). The magnitude of the negative-sequence output impedance at the system frequency. With respect to the parameter  $K_n$  for three values of  $\omega_{cut}$  is shown in Fig. 8. The maximum value of the parameter  $K_n$  is determined such that the stability margins of the closed-loop system are not degraded. The maximum value for  $Z_{out}(s)$ , or equivalently, the minimum permissible value for  $K_n$  can be calculated based on the IEEE standards [3], [4], i.e.,

$$\frac{V_{\alpha,\beta}^-}{V_{\alpha,\beta}^+} < 0.02 \Rightarrow \frac{Z_{out}^- I_{o_{\alpha,\beta}}^-}{V_{\alpha,\beta}^+} < 0.02. \quad (9)$$

Moreover, the capability of a VSC in injecting the negative-sequence current is a limiting factor which, together with (9),

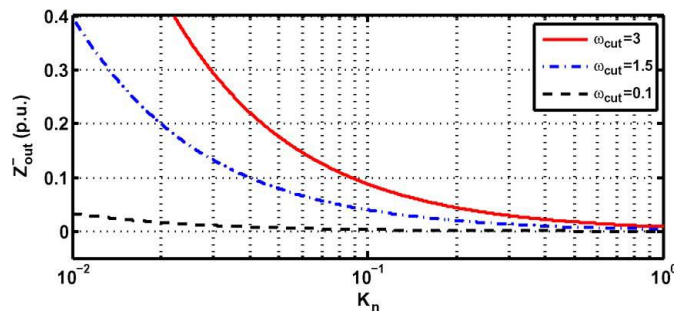


Fig. 8. Effect of  $K_n$  the negative-sequence output impedance of the inverter.

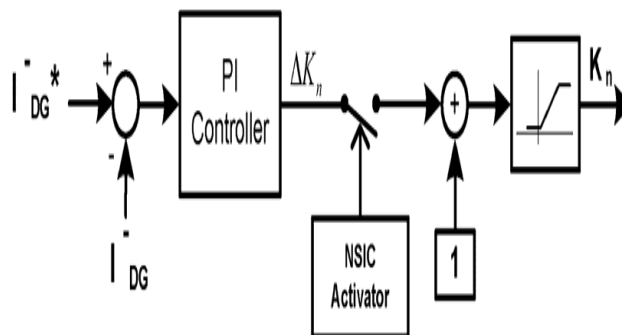


Fig. 9. NSIC structure

determine the maximum value of the negative-sequence output impedance. Fig. 9 shows the block diagram of the NSIC whose reference signal is

$$I_{DG}^{-*} = \sqrt{I_{loc}^{-2} + I_{nonloc}^{-+2} + 2I_{loc}^{-}I_{nonloc}^{-*} \cos \theta} \quad (10)$$

Where  $I_{loc}^{-}$ , is the negative-sequence current of the local load, is the phase difference between  $I_{loc}^{-}$  and  $I_{nonloc}^{-}$ :

$$I_{nonloc}^{-*} = \frac{I_{maxDG_i}^{-} I_{nonloc}^{-}}{\sum I_{maxDG_i}^{-}} \quad (11)$$

In(11),  $I_{maxdg}$ , is the maximum negative-sequence current that the  $i$ th DG can inject, and is the amplitude of the negative-sequence current of the feeder supplying the nonlocal loads. It should be noted that if the impedances of the MV lines from the nonlocal loads to the adjacent feeders supplied by the DGs are known, the negative-sequence of output impedance can be adjusted by parameter in an offline manner. However, to achieve optimal sharing of the negative-sequence current, it is required that the phasor of the negative-sequence current of each nonlocal load is measured and transmitted to all DG units. This can be performed by a low bandwidth communication link. In the context of the smart microgrids, the phase measurement units (PMUs) are used for this purpose. In the study system of Fig. 1, the PMUs are located at the 20-kV side of load transformers. One of the main advantages of the proposed method over the existing control strategies, i.e., [12]–[15], is that the phase-angle of the negative-sequence currents of the feeders are considered in the control loop. In some cases, therefore, the negative-sequence currents of the loads may cancel the effect of each other. In such cases, the DG units remain under balanced conditions. It should be noted that the NSIC is not always in service. When the NSIC is disabled, the negative-sequence output impedance of the DG is kept at its minimum, as indicated in Fig. 10. The flowchart of Fig. 10 determines when to activate the NSIC. According to this flowchart, the controller is enabled when 1) the capacity of a DG unit for injecting the negative-sequence current is reached, or 2) the local feeder with

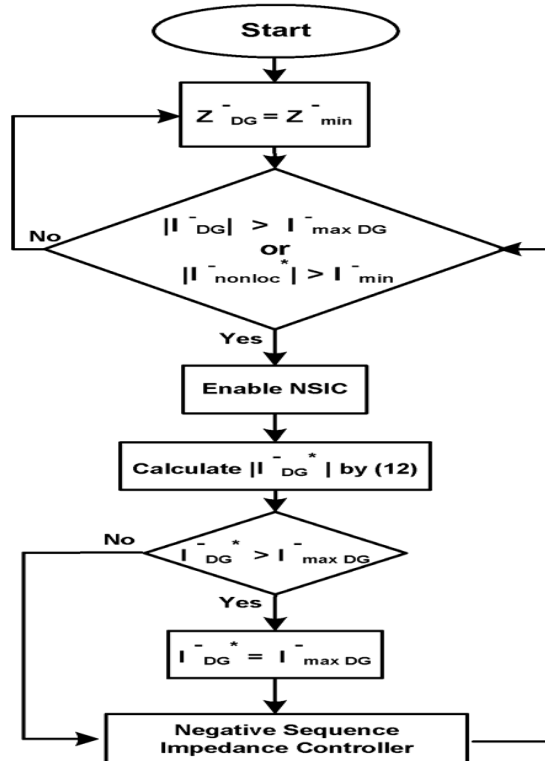


Fig. 10. Flowchart of negative-sequence current sharing strategy

Unbalanced load is not in an electrical proximity of a DG unit. Otherwise, the NSIC is disabled and the negative sequence of output impedance is kept constant at its minimum value. When the proposed NSIC is enabled, a PI controller adjusts the parameter to a desirable value. The PI controller is designed such that the NSIC closed-loop system has a low bandwidth. In this case, the coupling between the NSIC and other control loops will be minimized. Moreover, the NSIC is significantly slower than the droop and voltage controllers which prevents the undesirable transients in the microgrid.



## VI. Simulation Results

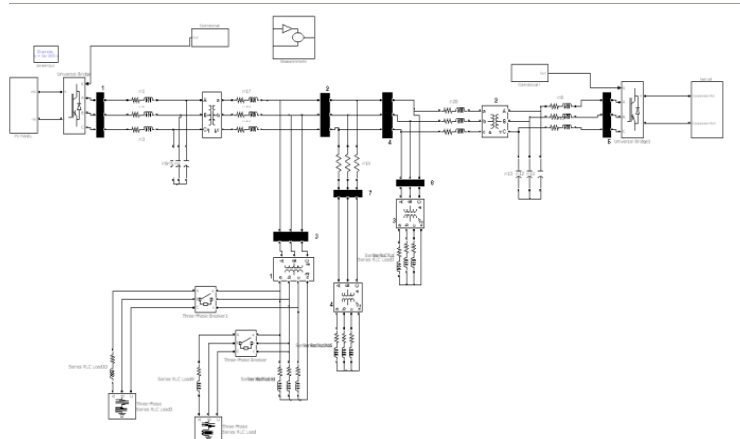


Fig :-MATLAB/SIMULINK MODEL OF FEEDER 1

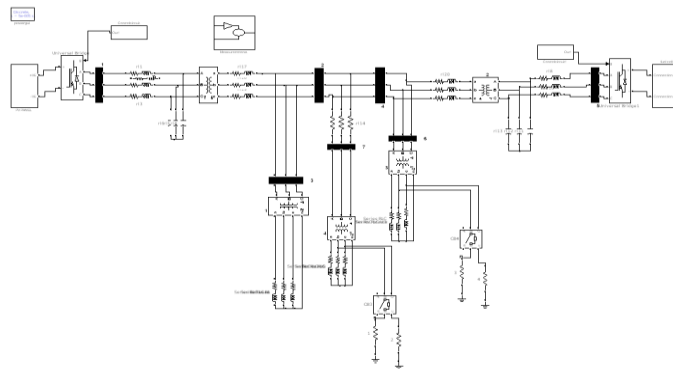
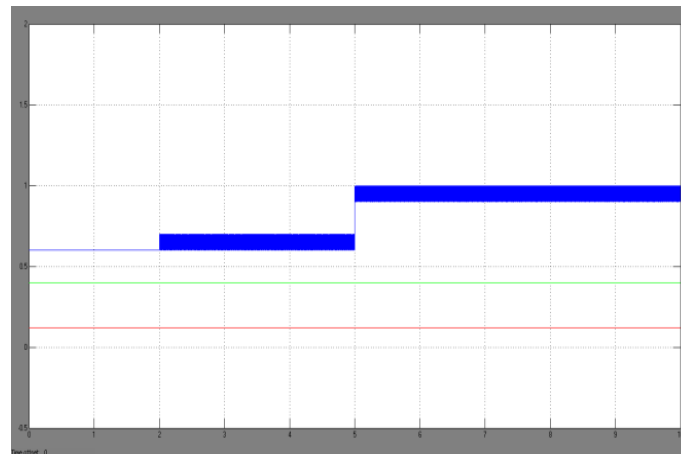


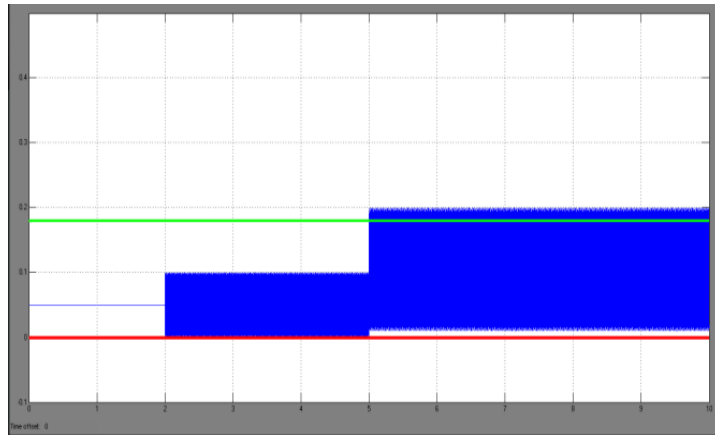
Fig :-MATLAB/SIMULINK MODEL OF FEEDER 2

The real and reactive power of the three feeders for these changes are shown in the below figure. Since feeder becomes unbalanced, a double-frequency ripple is appeared in the instantaneous power components of this feeder. As it is observed, the double-frequency ripple is increased at due to the inclusion of the unbalanced three-phase load. The figure below shows: Wave form for the Instantaneous Active power For Unbalanced Load Changes at Feeder F1



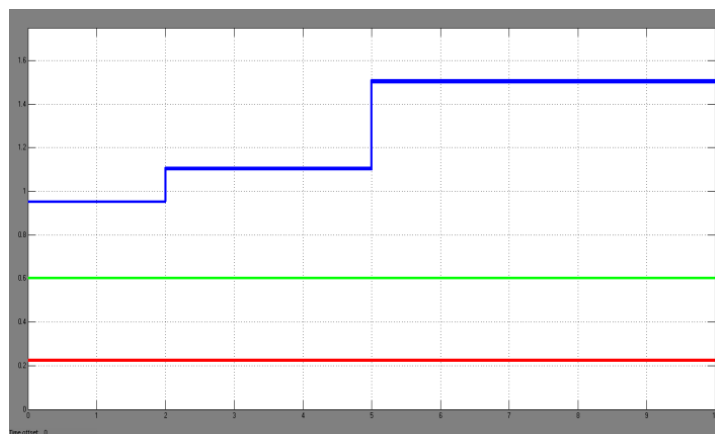
(a) Fig:- Wave form for the 3-phase instantaneous Active power For Unbalanced Load changes at feeder f1.

The figure below shows: Wave form for the Instantaneous Reactive power For Unbalanced Load Changes at Feeder F1



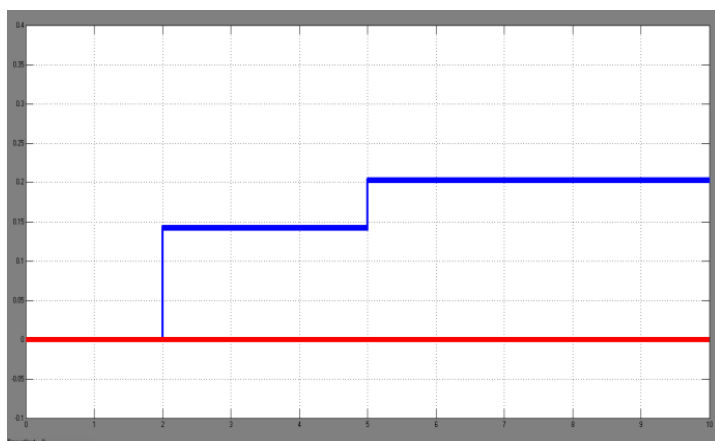
(b) Fig:- Wave form for the 3-phase instantaneous Reactive power For Unbalanced Load changes at feeder f1.

The figure below shows the positive- and negative-sequence components of the currents of all feeders. It is observed that the positive- and negative-sequence components step up at  $t=2s$  and  $t=5s$ . The figure below shows: Wave form for the Positive sequence currents for All feeders.



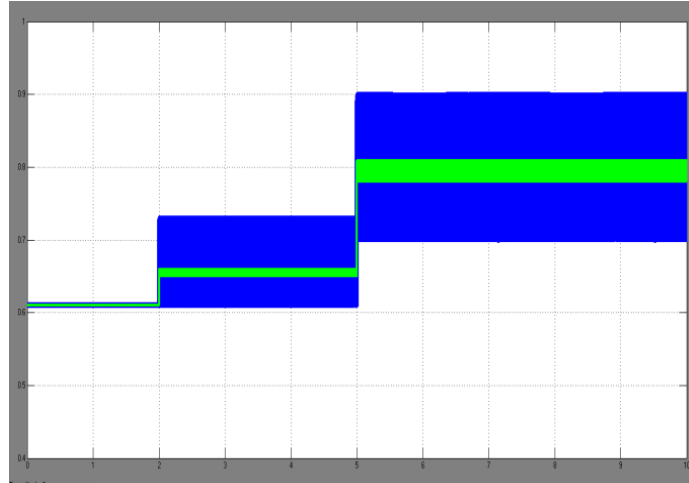
(a)Fig:- Wave form for the positive sequence currents for all feeders.

The figure below shows: Wave form for the Negative sequence currents for All feeders.



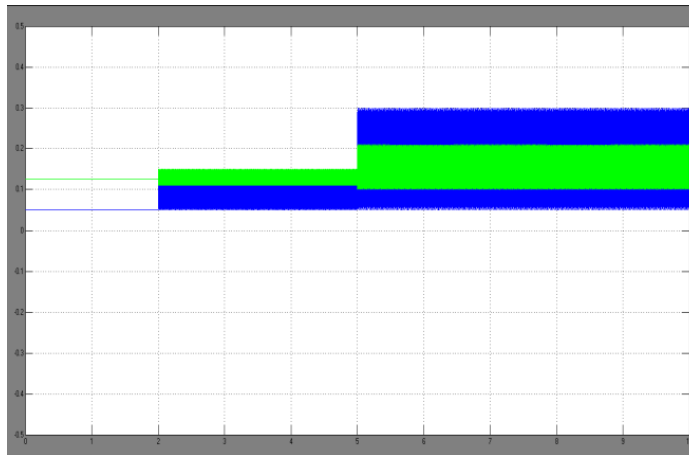
(b)Fig:- Wave form for the negative sequence currents for All feeders.

The figure below shows the instantaneous real and reactive power components of the DG units during the load switchings. The double-frequency ripple component of each DG is proportional to its negative-sequence currents. The simulation studies show that if the PR controller does not maintain the output impedance of the positive-sequence of each DG at the minimum value, the average power of the DG shows low frequency oscillatory transients. The figure below shows: Wave form for the Instantaneous Active power Of DG Units at feeder.



(a)Fig:- 3-phase Instantaneous Active Powers of DG Units at feeder f1.

The figure below shows: Wave form for the Instantaneous Reactive powers Of DG Units at feeder f1.



(b)Fig:- Wave form for the 3-phase Instantaneous Reactive Power Of DG Units at feeder f1.

Figs. 3(a&b) and 4(a&b) shows the instantaneous power components and the positive- and negative-sequence current components of the three feeders, respectively. Subsequent to the load switching event at  $t=2s$ , the DG units activate their NSICs to share the demanded negative-sequence current by feeder f3 after 0.9 s. In this case, the phasor of the NSIC is measured by a PMU and transmitted to the adjacent DG units. The reference signal of the NSIC of each DG unit is calculated. The figure below shows: Wave form for the Instantaneous Active power at feeder f1, f2 and f3.

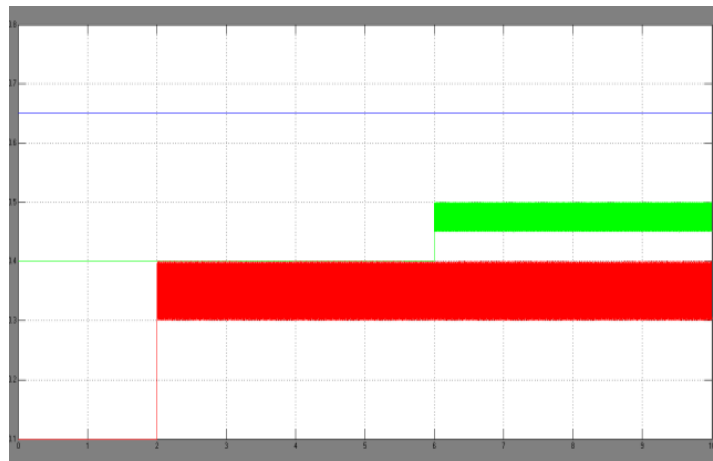


Fig 3(a):- Wave form for the 3-phase instantaneous Active power at f1, f2 and f3.

The figure below shows: Wave form for the Instantaneous Reactive power at feeder f1, f2 and f3.

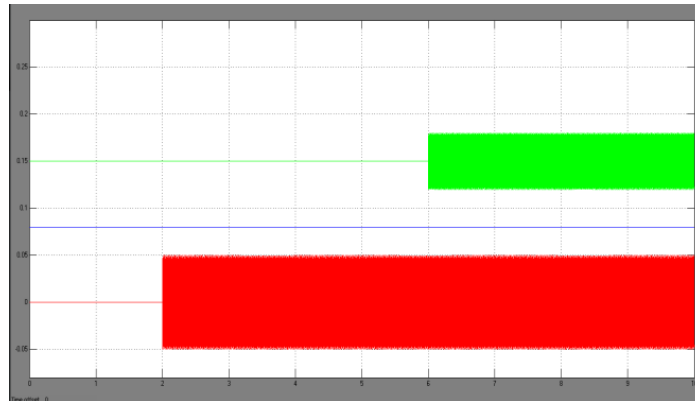


Fig 3(b) :- Wave form for the 3-phase instantaneous Reactive power at feeder f1, f2 and f3.

The figure below shows: Wave form for Positive sequence currents at feeder f1, f2 and f3

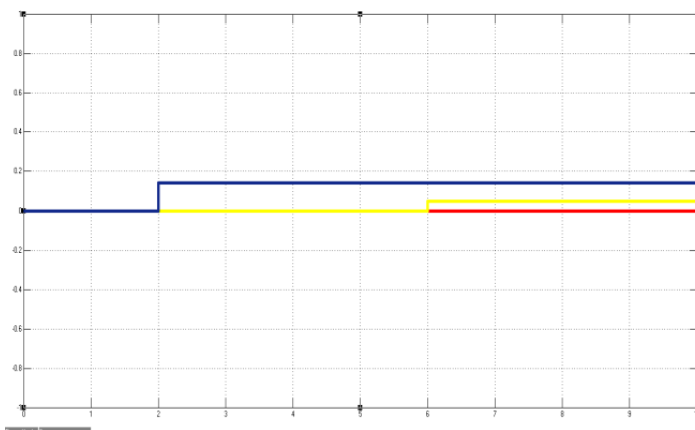


Fig 4(a):- Wave form for positive sequence currents at feeder f1, f2 and f3.

T

he figure below shows: Wave form for Negative Sequence currents at feeder f1, f2 and f3

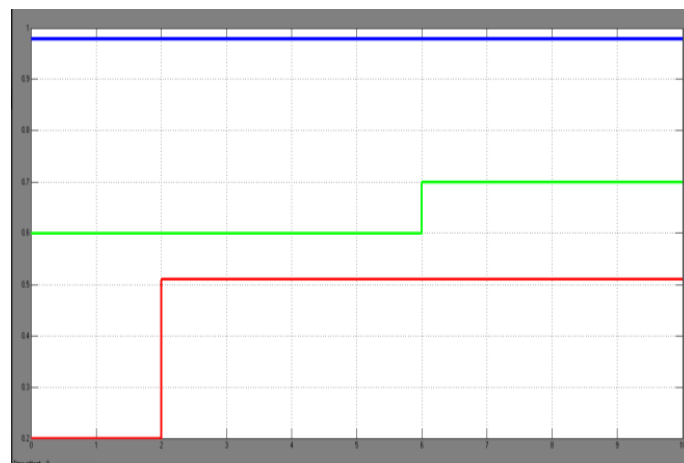


Fig4(b):- Wave form for negative sequence currents at feeder f1, f2 and f3

## VII. Conclusion

This paper presents a new control strategy for a multi-bus MV microgrid consisting of the dispatchable electronically-coupled DG units and unbalanced loads. The sources for the proposed system are selected as PV and Fuel cell. The negative-sequence current of a local load is completely compensated by its dedicated DG. However, the negative-sequence current of the nonlocal loads is shared among the adjacent DGs. The active and reactive powers are controlled efficiently by using the proposed control strategy. The simulation results conclude that the proposed strategy:

- robustly regulates voltage and frequency of the microgrid;
- is able to share the average power among the DGs;
- effectively compensates the negative-sequence currents of local loads; and
- shares the negative-sequence current of the nonlocal loads such that the power quality of the overall microgrid is not degraded.

## REFERENCES

- [1] N. Hatziargyriou, H. Asano, R. Iravani, and C. Marnay, "Microgrids," *IEEE Power Energy Mag.*, vol. 5, pp. 78–94, Jul.–Aug. 2007.
- [2] A. G. Madureira and J. A. P. Lopes, "Coordinated voltage support in distribution networks with distributed generation and microgrids," *IET Renew. Power Gener.*, vol. 3, pp. 439–454, Sep. 2009.
- [3] IEEE Recommended Practice for Monitoring Electric Power Quality, IEEE Std. 1159, 2009.
- [4] IEEE Recommended Practice for Electric Power Distribution for Industrial Plants, ANSI/IEEE Std. 141, 1993.
- [5] R. Lasseter, "Microgrids," in *Proc. IEEE Power Eng. Soc. Winter Meeting*, 2002, pp. 305–308.
- [6] M. H. J. Bollen and A. Sannino, "Voltage control with inverter-based distributed generation," *IEEE Trans. Power Del.*, vol. 20, no. 1, pp. 519–520, Jan. 2005.
- [7] M. C. Chandorkar, D. M. Divan, and B. Banerjee, "Control of distributed ups systems," in *Proc. 25th Annu. IEEE PESC*, 1994, pp. 197–204.
- [8] E. A. A. Coelho, P. C. Cortizo, and P. F. D. Garcia, "Small signal stability for parallel-connected inverters in stand-alone ac supply systems," *IEEE Trans. Ind. Appl.*, vol. 38, pp. 33–542, Mar./Apr. 2002.
- [9] N. L. Soutanis, A. I. Tsouchnikas, N. D. Hatziargyriou, and J. Mahseredjian, "Dynamic analysis of inverter dominated unbalanced lv micro-grids," *IEEE Trans. Power Syst.*, vol. 22, no. 1, pp. 294–304, Feb. 2007.
- [10] Y. Li, D. M. Vilathgamuwa, and P. C. Loh, "Design, analysis, and realtime testing of a controller for multibus microgrid system," *IEEE Trans. Power Electron.*, vol. 19, pp. 1195–1204, Sep. 2004.
- [11] T. L. Lee and P. T. Cheng, "Design of a new cooperative harmonic filtering strategy for distributed generation interface converters in an islanding network," *IEEE Trans. Power Electron.*, vol. 22, pp. 1919–1927, Sep. 2007.
- [12] P. Cheng, C. Chen, T. Lee, and S. Kuo, "A cooperative imbalance compensation method for distributed-generation interface converters,"
- [13] M. B. Delghavi and A. Yazdani, "Islanded-mode control of electronically coupled distributed-resource units under unbalanced and nonlinear load conditions," *IEEE Trans. Power Del.*, vol. 26, no. 2, pp. 661–673, Apr. 2011.
- [14] D. De and V. Ramanarayanan, "Decentralized parallel operation of inverters sharing unbalanced and non-linear loads," *IEEE Trans. Power Electron.*, vol. 25, pp. 3015–3025, Aug. 2010.
- [15] R. Majumder, A. Ghosh, G. Ledwich, and F. Zare, "Load sharing and power quality enhanced operation of a distributed microgrid," *IET Renew. Power Gener.*, vol. 3, no. 2, pp. 109–119, 2009.
- [16] M. N. Marwali and A. Keyhani, "Control of distributed generation systems- part i: Voltages and currents control," *IEEE Trans. Power Electron.*, vol. 19, pp. 1541–1550, Nov. 2004.
- [17] A. Timbus, M. Liserre, R. Teodorescu, P. Rodriguez, and F. Blaabjerg, "Evaluation of current controllers for distributed power generation systems," *IEEE Trans. Power Electron.*, vol. 24, pp. 654–664, Mar. 2009.
- [18] H. Karimi, A. Yazdani, and R. Iravani, "Robust control of an autonomous four-wire electronically-coupled distributed generation unit," *IEEE Trans. Power Del.*, vol. 26, no. 1, pp. 455–466, Jan. 2011.
- [19] H. Akagi, E. H. Watanabe, and M. Aredes, *Instantaneous Power Theory and Applications to Power Conditioning*. New York: Wiley, 2007.
- [20] M. C. Chandorkar, D. M. Divan, and R. Adapa, "Control of parallel connected inverters in standalone ac supply systems," *IEEE Trans. Ind. Appl.*, vol. 29, no. 1, pp. 136–143, Jan.–Feb. 1993.
- [21] M. Karimi-Ghartemani and H. Karimi, "Processing of symmetrical components in time-domain," *IEEE Trans. Power Syst.*, vol. 22, no. 2, pp. 572–579, May 2007.



Mr. T. Venugopal is currently Associate Professor in the Department of Electrical and Electronics Engineering, Vaagdevi college of engineering, Warangal, India. He graduated and also pursued M.Tech from JNTUH his area of interests include Energy management, Distributed Generation, power electronics in volvemachine drives and power systems etc,



Mr.B.Bhavsingh is currently assistant professor in the Department of Electrical and Electronics Engineering, Jayamukhi Institute of Technological Sciences, Warangal. He received the M.Tech Degree in Power Electronics From Vaagdevi College of Engineering, Warangal, in 2012. He has teaching Experience Of 3 yrs in SRR and Jayamukhi Institute Of Technological Sciences (JNTUH), Warangal A.P His Interests Include DG's, Microgrids And Renewable energy resources.



**D.Vani** received the B.Tech Degree in Electrical And Electronics Engineering From NIGAMA Engineering college (JNTUH), Karimnagar, A.P in 2012. He is currently pursuing the M.Tech Degree in Power Electronics in Vaagdevi College of Engineering (JNTUH), Warangal A.P and Interests Include DG's, Microgrids And Power electronics Operation And Control